Plasma Chem Plasma Process (2016) 36:1559–1570
DOI 10.1007/s11090-016-9739-9

ORIGINAL PAPER

Comparison of the Active Species in the RF and Microwave Flowing Discharges of N_2 and Ar–20 %N_2

André Ricard[1,2] · Jean-Philippe Sarrette[1,2] · Soo-Ghee Oh[3] · Yu Kwon Kim[3]

Received: 9 March 2016 / Accepted: 28 July 2016 / Published online: 8 August 2016

Abstract We report a detailed comparison between RF and microwave (HF) plasmas of N_2 and Ar–20 %N_2 as well as in the corresponding afterglows by comparing densities of active species at nearly the same discharge conditions of tube diameter (5–6 mm), gas pressure (6–8 Torr), flow rate (0.6–1.0 slm) and applied power (50–150 W). The analysis reveals an interesting difference between the two cases; the length of the RF plasma ($\sim$25 cm) is measured to be much longer than that of HF (6 cm). This ensures a much longer residence time (10^{-2} s) of the active species in the N_2 RF plasma [compared to that (10^{-3} s) of HF], providing a condition for an efficient vibrational excitation of $N_2(X, v)$ by (V–V) climbing-up processes, making the RF plasma more vibrationally excited than the HF one. As a result of high V–V plasma excitation in RF, the densities of the vibrationally excited $N_2(X, v > 13)$ molecules are higher in the RF afterglow than in the HF afterglow. Destruction of $N_2(X, v)$ due to the tube wall is estimated to be very similar between the two system as can be inferred from the γ_v destruction probability of $N_2(X, v > 3–13)$ on the tube wall (2–3 $\times$ 10^{-3} for both cases) obtained from a comparison between the density of $N_2(X, v > 3–9)$ in the plasmas to that of the $N_2(X, v > 13)$ in the long afterglows. Interestingly enough, densities of N-atoms and $N_2(A)$ metastable molecules in the afterglow regions, however, are measured to be very similar with each other. The measured lower density of N_2^+ ions than expected in the HF afterglow is rationalized from a high oxygen impurity in our HF setup since N_2^+ ions are very sensitive to oxygen impurity .

Keywords N_2 RF and HF plasmas · N_2 RF and HF afterglows · N density · $N_2(A)$ and $N_2(X, v > 13)$ density · N_2^+ density · Wall destruction probability

✉ André Ricard
ricard@laplace.univ-tlse.fr

[1] UPS, INP, LAPLACE (Laboratoire Plasma et Conversion d'Energie), Université de Toulouse, 118 route de Narbonne, 31062 Toulouse, France

[2] LAPLACE, CNRS, 31062 Toulouse, France

[3] Department of Energy Systems Research, Ajou University, Suwon 443-74, Korea

Introduction

N_2 plasmas and corresponding afterglows have been intensively studied [1–5] with an interest in utilizing excited nitrogen species in various applications such as plasma sterilization [6–8], plasma cleaning [9–11] and surface nitridation [12–14]. Under a controlled flowing condition, an inherent nature of a longer lifetime of a certain excited N_2 species makes it possible to obtain an 'afterglow' region with a varying density of N-atoms, $N_2(X, v > 13)$ and $N_2(A)$ metastable molecules and N_2^+ ions [1]. This condition may provide a chance of developing a 'damage-free' plasma process in diverse application fields [7, 14].

In this respect, the exact determination of active species density in the plasma as well as in the afterglow would be a first step toward a successful use of them in application. RF and microwave (HF) plasmas in N_2 and Ar–N_2 have been previously studied and the detailed densities of active species in the afterglow under a flowing condition have been carefully measured at two different locations of Ajou University and University of Toulouse [1, 2]. The densities of N-atoms, $N_2(X, v > 13)$ and $N_2(A)$ metastable molecules and N_2^+ ions were determined using the line ratio method [1, 15] and the calibration of the N-atom density by NO titration [3, 4, 16]. These recent studies revealed important characteristics of the two plasma systems, especially in terms of plasma length, plasma temperatures and the changing densities of active species in the plasmas and the afterglows, which were explained as a result of complex kinetic processes of the active species in the N_2 plasmas [1, 2, 4, 5, 16–21]. Recently, we have also reported detailed variation of active species in the RF plasmas and their afterglows of N_2 and Ar–20 %N_2 [5]. Despite such vast reports on the detailed characteristics of the N_2 and Ar–N_2 plasmas, a comprehensive comparison of plasma systems with different sources of plasma power (such as RF and HF) is still missing in the literature, while it can be an invaluable information for choosing the right source of plasma power in specific applications such as medical instruments sterilization [7] and iron nitriding [14] in N_2 afterglows. Luckily enough, we have accumulated enough experimental data set for a quantitative comparison of the two plasma systems of RF and HF for the case of N_2 plasma obtained under very similar flowing conditions. Based on this motivation, here we present our recent analysis on the differences between the two plasmas (RF and HF) and their afterglows in terms of plasma rotational and vibrational temperatures and densities of the active nitrogen species in the respective afterglows of mixed pink afterglow (PA) and late afterglow (LA). The afterglows are compared at the residence times of 7×10^{-2} s for the RF and 10^{-3} to 6×10^{-2} s for the HF. We also report the destruction probability of vibrationally excited $N_2(X, v)$ molecules on the RF and HF afterglow tube walls.

Experimental Setups

The two experimental setups of RF and HF plasmas in Ajou and Toulouse, respectively, are reproduced in Fig. 1 for comparison.

The discharge quartz tubes have nearly the same inner diameters (ID) of 6 mm for the RF plasma reactor and 5 mm for the HF plasma reactor and have a length of 30 cm in both cases. In the post-discharge region, the RF discharge tube is connected to a straight quartz tube of 21 mm ID while the HF discharge tube is connected to a bent quartz tube of 18 mm ID itself connected to a 5 L-Pyrex chamber (Fig. 1). For both systems, experiments were conducted at very similar operation conditions of pressure (8 Torr), flow rate (0.5–1.0 slm)

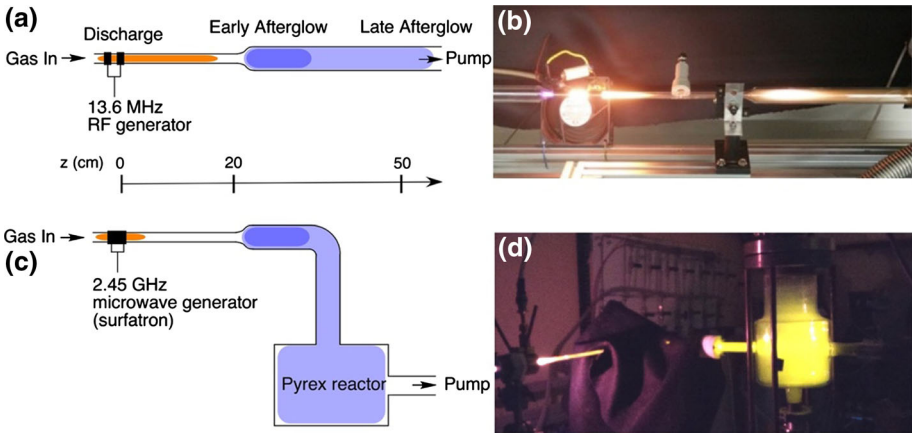

Fig. 1 Schematic diagrams and their pictures of the RF (**a**, **b**) and the HF (**c**, **d**) set-ups in Ajou and Toulouse, respectively, are shown. In the RF (HF) set-up, the inner diameters of the quartz tubes are 6 (5) mm in the discharge region and 21 (18) mm in the afterglow region

and applied power (50–150 W). The emission spectra across the RF reactor are obtained by means of a spectrometer (Monera 500, resolution 0.2–0.8 nm) with a PMT (Hamamatsu R928) using an optical fiber [1]. Across the HF reactor, an optical fiber is connected to an Acton Spectra Pro 2500i spectrometer (grating 600 g/mm) equipped with a Pixis 256E CCD detector (front illuminated 1024 × 256. The above similarities in the geometry of the two plasma systems allow us to compare the two RF and HF plasmas and afterglows to further understand the inherent differences in the type of plasma between the two plasmas. Plasmas are investigated by emission spectroscopy by measuring emission between the two rings of the RF discharge for the case of RF plasma and near the gap of the surfatron cavity (with a spatial resolution estimated to be 5 mm) for the case of HF plasma, respectively. N_2 second positive (2nd pos), N_2^+ first negative (1st neg) and N_2 first positive (1st pos) intensities are recorded at these two positions.

The N_2 and Ar–N_2 RF and HF Plasmas

In the same ranges of gas pressure (6–8 Torr), flow rate (0.6–1.0 slm) and power (50–100 W), it is observed that the plasma region, defined as the most luminous glow downstream of the RF coils and HF gap, respectively, is longer in RF than in HF. For pure N_2, the HF plasma length (L_p) at 8 Torr increases from 1 to 6 cm when the power is increased from 50 to 100 W, while in the RF plasma, L_p varies from 18 to 25 cm for the same power variation. Such an increase of L_p of 2.45 GHz microwave plasmas in HF cavity at 100–140 W has been effectively observed in N_2 plasma at 30 Torr with L_p increasing from 2.5 to 8 cm [13]. The difference is even more pronounced in Ar–x %N_2 gas mixtures in which L_p increases with increasing Ar ratio. L_p is longer than the tube length (30 cm) for the RF plasma in Ar–x %N_2 when x is lower than 20 %. With the HF plasma, it is even possible to decrease x down to 2 % since the HF plasma length is still confined in the tube of 30 cm length. Thus, the comparison between RF and HF is presently limited to results in pure N_2 and in the Ar–20 %N_2 gas mixture.

For low pressure plasmas, it is known that the (minimum) cut-off electron density required to maintain a surface wave discharge depends on the square of the frequency (f^2) of the electro-magnetic wave transferring the energy to the gas [22]. It is mentioned that the f^2 variation of electron density at the plasma end is given in [22] for Ar surface wave plasma at pressure less than 1 Torr. It is extended here to the present RF (13.6 MHz) and HF (2450 MHz) plasma columns to explain our observation that the length of the RF plasma is longer than the HF one at a same gas pressure and transmitted power.

The plasma length (L_p) is of crucial importance for the $N_2(X, v)$ excitation by the electron–vibration (e–V), vibration–vibration (V–V) and vibration–translation (V–T) processes as previously reported and applied to results of a N_2 DC flowing discharge [23]. At the end of the RF plasma ($L_p = 30$ cm, 100 W), the residence time (t_R) is 10^{-2} s, one order of magnitude higher than at the end of the HF plasma where $t_R = 8 \times 10^{-4}$ s ($L_p = 6$ cm, 100 W). As a consequence, the (V–V) processes are more developed in the RF plasma than in HF one.

The Plasma Gas Temperature

The intensity ratio (P1/P2) of the first two rotational sub-bands (labelled as P1 and P2) of the 1st pos N_2 band at 775 nm is related to the rotational temperature (T_R) of the plasma which is usually between 300 and 1000 K [19]. It is an important characteristic parameter of the N_2 plasma since it is directly related to the gas temperature (T_g), due to the efficient rotational-translational energy transfer. It is found that with an applied power between 50 and 100 W, the RF plasma at 6–8 Torr and 0.5–0.6 slm is a little warmer ($T_g = 500$–800 K) than the HF plasma at 8 Torr, 1 slm where $T_g = 500$–600 K. The uncertainty of gas temperature measurements is estimated to be 20 % [19].

The Plasma Vibrational Temperature

The vibrational temperatures can be analyzed from the intensity ratios of the N_2 2nd pos. sequence $\Delta v = -2$ as detailed in [19]. The vibrational $T_V(C)$ and characteristic θ_1-(X) temperatures, corresponding to the excited $N_2(C\ ^3\Pi_u)$ and $N_2(X\ ^1\Sigma_g^+)$ ground states, respectively, are connected to each other as can be seen from the following two steps:

First, the $f(v)$ vibrational distribution of $N_2(X, v)$ is expressed as follows [24]:

$$f(v) = f(0) \cdot \exp^{-v\left(\frac{E_{10}}{\theta_1(x)} - \frac{(v-1)E_{10}\delta}{Tg}\right)} \tag{1}$$

with $f(0) = 1 - \exp^{-\frac{E_{10}}{\theta_1(x)}}$ for $v < v_T$, where v_T is the vibrational number of the Treanor minimum given by $v_T = \frac{T_g}{2\delta\theta_1(X)} + 0.5$, E_{10} is the energy difference between the first two vibrational levels E(X, 1)–E(X, 0) (in K) and δ is the anharmonicity constant.

For $N_2(X)$, $E_{10} = 3396$ K and $\delta = 6.22 \times 10^{-3}$.The population of $N_2(X, v)$ is then written as $[X, v] = f(v)\ N_0$, where N_0 is the N_2 density.

Second, by considering that the $N_2(C, v')$ states are mainly produced by electron collisions on the $N_2(X, v)$ ground states, following the Franck–Condon principle (vertical direct excitation by electron collisions), the stationary $[C, v']$ population is written as follows:

$$[C, v'] = \Sigma_v [X, v]\ n_e k_e(C)\ q(X, v - C, v')/v(C, v') \tag{2}$$

where $q(X, v–C, v')$ is the Franck–Condon factor [24], n_e is the electron density, $k_e(C)$ is

the electron excitation rate which depends on the electron excitation cross-sections and on the electron energy distribution and $\nu(C, v') = \nu_R(C, v') + N_0\, k_Q(C, v')$, ($\nu_R(C, v')$ and $k_Q(C, v')$ are the radiative loss frequency [25] and the collisional quenching rate by the N_2 molecules [26]), respectively. The thresholds between the $N_2(C, v' = 0–3)$ and the $N_2(X, v = 0–8)$ varying from 9 to 11.5 eV and the value of $k_e(C)$ is approximated to be constant [27]. For the pressure range used in the present work, $N_0\, k_Q(C, v')$ can be neglected in front of $\nu_R(C, v')$.

As previously described [19], the experimental relative distribution $[C, v' < 4]$ is obtained by measuring the band head intensities of the N_2 2nd pos. sequence $\Delta v = -2$. If a Boltzmann distribution of $[C, v']$ is verified, the vibrational temperature $T_V(C)$ can be obtained.

The vibrational distribution of the N_2 ground state $[X, v]$ and the corresponding vibrational temperature $\theta_1(X)$ are obtained from the experimental values of T_g and of the $[C, v' < 4]$ distributions by combining Eqs. (1) and (2).

Figure 2 shows the calculated$[C, v' < 4]$ distributions normalized to $[C, v' = 0]$ for the $\theta_1(X)$ values of 5, 8 and 20×10^3 K which are compared with the experimental determined values ($[C, v' < 4]/[C, v' = 0]$) for the RF and HF plasmas. From the comparison, $\theta_1(X) = 8 \times 10^3$ K and $\theta_1(X) = 5 \times 10^3$ K are chosen for the RF and HF plasmas, respectively. Note that the $[C, v' < 4]$ calculated distributions have been found to be weakly influenced by the T_g variations between 500 and 800 K. It is observed a high value of the $N_2(C, v = 1)$ density of the RF plasma which has been previously interpreted as a result of collisions between electrons and the $N_2(A)$ metastable molecules [27, 28].

Table 1 reproduces the values of T_g (see "The plasma gas temperature" section), $\theta_1(X)$, v_T and $N_2(X, v = v_T)$ for the N_2 and Ar–20 %N_2 plasmas at 6 Torr, 100 W for RF where $[N_2]_{RF} = 7 \times 10^{16}$ cm^{-3} and at 8 Torr, 100 W for HF where $[N_2]_{HF} = 1.5 \times 10^{17}$ cm^{-3}.

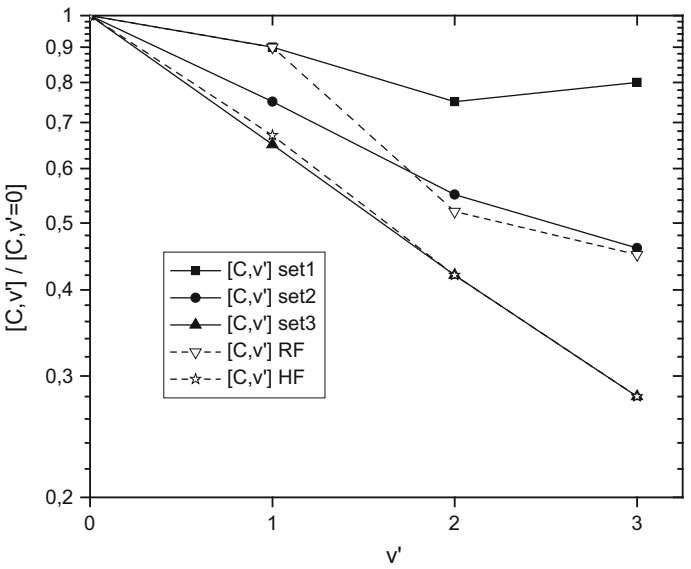

Fig. 2 Vibrational distributions of $N_2(C, v' < 4)$ versus v' for set1 $[\theta_1(X) = 2 \times 10^4$ K], set2 $[\theta_1(X) = 8 \times 10^3$ K] and set3 $[\theta_1(X) = 5 \times 10^3$ K]. The experimental points are *triangles* for RF and *stars* for HF

Table 1 Values of T_g, $T_v(C)$, $\theta_1(X)$, v_T and $N_2(X, v = v_T)$ for the RF plasma at 6 Torr, 100 W and for the HF plasma at 8 Torr, 100 W

Plasma gas	Discharge type	T_g (K)	$\theta_1(X)$ (10^3 K)	v_T	$N_2(X, v = v_T)$ (10^{15} cm^{-3})
N_2	RF	800	8	9	4
N_2	HF	500	5	8–9	3
Ar–20 %N_2	RF	700	8	7	0.9
Ar–20 %N_2	HF	600	6	8	0.8

We find a higher $\theta_1(X)$ temperature in RF than in HF. This result agrees well with our suggestion of a more vibrationally excited RF plasma than the HF one.

The N_2 and Ar–20 %N_2 RF and HF Afterglows

Afterglows Characteristics

Characteristics of the afterglows can be studied by measuring the emission bands of N_2 1st pos. (chosen band at 580 nm), N_2 2nd pos. (chosen band at 316 nm) and N_2^+ 1st neg. (chosen band at 391.4 nm).

The analysis of the N_2 1st pos. vibrational distribution reveals that the N_2 afterglows are a mixture of pink (PA) and late (LA) afterglows. In a pure LA, the 1st pos. emission is only due to the 3 body recombination of nitrogen atoms. To evaluate the contribution of the LA emission ($a_{N+N} = 1$ for pure LA and $a_{N+N} = 0$ for pure PA), the a_{N+N} value is obtained from a comparison between experimental and theoretical vibrational intensities distributions of the $\Delta v = -4$ sequence (see [1–4, 16]).

For the experimental conditions of 8 Torr, 0.5 slm and 100 W in the RF set-up with the tube ID of 21 mm at z = 34 cm (see Fig. 1), a pure N_2 PA is observed. It is followed by an increasing contribution of the LA with increasing z. At z = 51 cm (17 cm downstream from the starting point of the 21 mm quartz tube), the a_{N+N} value of 0.5 is obtained at the same experimental conditions.

For the HF afterglow, a_{N+N} of 0.3 is obtained at 3 cm downstream from the starting point of the 18 mm quartz tube (z = 18 cm, Fig. 2) at 8 Torr, 1 slm and 150 W. It increases up to 0.8 at z = 55 cm. In this case, a pure LA is obtained just before the 5 L-reactor (see Fig. 1).

The measured larger z values for the RF afterglows (the mixed PA and LA of $0 < a_{N+N} < 1$) than for the HF indicate longer afterglow times. For the RF afterglow, it is calculated to be 7×10^{-2} s at z = 51 cm (Fig. 1) by assuming a laminar flow in the 21 mm quartz tube.

As for the HF afterglow, it is estimated to be 1.5×10^{-3} s at z = 18 cm (Fig. 2) for a post-discharge jet with low radial expansion having the same gas velocity than in the discharge tube of 5 mm ID, as calculated in [29]. At z > 20 cm, a laminar flow is assumed in the tube of dia. 18 mm, giving a residence time of 6×10^{-2} s at z = 55 cm.

Densities of N, $N_2(A)$, $N_2(X, v > 13)$ and N_2^+

In the LA ($a_{N+N} = 1$), the N-atoms recombine as follows [1–4, 16]:

$$\begin{aligned} N + N + N_2 &\rightarrow N_2(B, 11) + N_2 \\ N_2(B, 11) &\rightarrow N_2(A, 7) + hv(580\,nm) \end{aligned} \quad (a)$$

When $a_{N+N} < 1$ (that is, a mixture of LA and PA), the a_{N+N} fraction of the measured I_{580}^m intensity can be related to the square of the N-atom density as follows:

$$a_{N+N} I_{580}^m = k_3 [N]^2 \quad (3)$$

The calibration coefficient k_3 is obtained by the use of NO titration, which also gives an independent access to the N-atom density.

In the RF N_2 plasma, it is found that the N-atom density slowly increases from 1 to 2×10^{15} cm^{-3} as the RF power increases from 50 to 130 W under the condition of 8 Torr, 0.5 slm and z = 51 cm (residence time of 7×10^{-2} s) where $a_{N+N} = 0.5$. In Ar–20 %N_2, the N-atom density is about 2×10^{15} cm^{-3} at 10 – 50 W.

For the HF case (see Table 2), the N-atom density slowly increases from 1.0 to 1.2×10^{15} cm^{-3} for the residence times between 1.5×10^{-3} and 6×10^{-2} s. Thus, it can be concluded that the N-atom density is about the same in the afterglow regions after the RF and HF plasmas considering the uncertainty on N-atom density to be 30 % [4].

Densities of the other active species ($N_2(A)$, $N_2(X, v > 13)$ and N_2^+) are then obtained by the line-ratio method as developed in [1].

For the $N_2(A)$ density determination, the main $N_2(C)$ excitation is considered from the following pooling reaction:

$$\begin{aligned} N_2(A) + N_2(A) &\rightarrow N_2(C, v = 1) + N_2 \\ N_2(C, v = 1) &\rightarrow N_2(B, v = 0) + N_2 2nd\ pos\ (316\,nm) \end{aligned} \quad (b)$$

Then, the following line–ratio is considered:

$$a_{N+N} I_{580}^m / I_{316}^m = k_4 ([N]/[N_2A])^2 \quad (4)$$

The k_4 coefficient is calculated from the rate coefficients of reactions (a) and (b) as reported in [1–4, 16] for the two RF and HF studied afterglows.

Table 2 Active specie densities and γ_v values after the N_2 HF and RF plasmas at 8 Torr, 1–0.5 slm and 100 W at various afterglow times

	HF				RF
Afterglow time (10^{-3} s)	1.5	20	35	60	70
a_{N+N}	0.3	0.55	0.45	0.8	0.5
N (10^{15} cm^{-3})	1.0	1.1	1.1	1.2	2
$N_2(A)$ (10^{11} cm^{-3})	1–5	1	1–2		2
$N_2(X, v > 13)$ (10^{13} cm^{-3})	6–10	8	7		20
N_2^+ (10^8 cm^{-3})	0.2–1.4	0.2	0.4		20
γ_v		5×10^{-3}	3×10^{-3}		2×10^{-3}

It is concluded that a nearly constant value of $[N_2(A)] = 1–2 \times 10^{11}$ cm^{-3} is obtained as the RF power increases from 50 to 100 W in N_2 and from 10 to 50 W in Ar–20 %N_2 at the residence time of 7×10^{-2} s.

The $N_2(A)$ density at the residence time of 1.5×10^{-3} s is $1–5 \times 10^{11}$ and 5×10^{12} cm^{-3}, respectively, after the N_2 and Ar–20 %N_2 HF plasmas under the condition of 8 Torr, 1 slm and 100–150 W. As shown in Table 2, the $N_2(A)$ density is nearly constant for the residence times up to 3.5×10^{-2} s. By this method, the $N_2(A)$ density is estimated to be in the range 10^{11}–10^{12} cm^{-3}.

Then, the $N_2(X, v > 13)$ density is deduced by considering that the $N_2(B, v = 11)$ state in the PA is produced by the following main reaction:

$$N_2(A) + N_2(X, v > 13) \rightarrow N_2(B, v = 11) + N_2(X) \quad (c)$$

The ratio of $a_{N+N}\, I^m_{580}$ (LA) and $(1 - a_{N+N})\, I^m_{580}$ (PA) is as follows:

$$(a_{N+N}/\,1 - a_{N+N})\,[A]\,[X, v > 13]\; k_c = [N]^2 k_a [N_2] \quad (5)$$

Here, the $N_2(X, v > 13)$ density is determined from a_{N+N} values, the N-atoms and the $N_2(A)$ densities.

A nearly constant $[N_2(X, v > 13)]$ density of $1–2 \times 10^{14}$ cm^{-3} is obtained at 50–100 W for pure RF N_2 and at 10–50 W for the Ar–20 %N_2 gas mixture.

At the residence time of 1.5×10^{-3} s after the HF plasma (8 Torr, 1 slm and 100 – 150 W), the $[N_2(X, v > 13)]$ density is $5–6 \times 10^{13}$ cm^{-3} for both N_2 and Ar–20 %N_2.

Such $[N_2(X, v > 13)]$ density can be considered as an estimated value which can vary depending on the k_c rate coefficient.

The measured N-atoms and $N_2(X, v > 13)$ densities above are in the same order of magnitude with the values reported in [14] in which $[N_2(X, v > 4)] = 3 \times 10^{13}$ cm^{-3} and $[N] = 6 \times 10^{14}$ cm^{-3} are obtained in N_2 and Ar–N_2 afterglow of HF plasmas at 7 Torr, 3 slm and 200 W.

It should be noted that the $N_2(X, v > 13)$ densities found in the present RF and HF afterglows are about one order of magnitude lower than the $N_2(X, v = 7–9)$ densities in the corresponding plasmas (see Table 1). This result is used to determine the rate of destruction of these vibrational molecules on the tube wall in the following section.

For the N_2^+ ions, the following dominant reactions in PA are considered [1]:

$$N_2(a') + N_2(a') \rightarrow e + N_2^+(X) + N_2(X) \quad (d)$$

$$\begin{aligned} &N_2^+(X) + N_2(X, v > 12) \rightarrow N_2^+(B) + N_2(X) \\ &N_2^+(B, 0) \rightarrow N_2^+(X, 0) + h\nu(391\,\text{nm}) \end{aligned} \quad (e)$$

where reaction (d) is for the Penning ionization in the afterglow and reaction (e) indicates the excitation of $N_2^+(X)$ by vibrational molecules $N_2(X > 12)$.

The N_2^+ density is deduced from the $N_2(X, v > 12)$ and $N_2(A)$ densities by considering the line-ratio I_{391}/I_{316} from reactions (e) and (b):

$$I_{391}/I_{316} = k_5\left(\left[N_2^+\right]\,[N_2(X, v > 12)]/[N_2(A)]^2\right), \quad (6)$$

The k_5 coefficient is calculated from the rate coefficients of reactions (e) and (b) [4, 16].

By taking $[N_2(X), v > 12] = [N_2(X), v > 13]$, it is found that the N_2^+ density increases from 5×10^8 to 2×10^9 cm^{-3} for the case of the RF N_2 plasma, when the RF power is

raised from 70 to 100 W. In Ar–20 %N_2 RF gas mixture, the N_2^+ ion density remains at 5×10^8 cm^{-3} at 10–50 W. After the HF afterglows, the N_2^+ density is in the range $(0.2–1.4) \times 10^8$ cm^{-3} as reported in Table 2.

The observed strong variations of the N_2^+ density originate from the fact that it is very sensitive to air impurity. By applying the intensity line-ratio method in comparison of I_{320} of the NO_β band to a_{N+N} I_{580}, an O-atom density of 9×10^{12} cm^{-3} (that is, 30 ppm at 8 Torr) and N_2^+ density of 10^9 cm^{-3} have been previously determined in the RF afterglow [1]. In the HF afterglow, the O-atom density is in the order of 10^{14} cm^{-3} (that is, 400 ppm or 4×10^{-4} [O]/[N_2] ratio) and the N_2^+ density is 10^8 cm^{-3}. These results clearly show that N_2^+ ions produced in the afterglow by the Penning ionization $N_2(a') + N_2(a')$ reaction are strongly correlated to the amount of O-atom impurity.

Destruction Probability of N_2(X, v > 3–13) on the Tube Walls

Densities of the N_2(X, $v > 3$) vibrational levels are found to be of 3 and 4×10^{15} cm^{-3} in the respective RF and HF plasmas and about 10^{14} cm^{-3} for N_2(X, $v > 13$) in the afterglows. By assuming a "plateau" of N_2(X, $v > v_T$), which means that a nearly constant vibrational density is reached after the Treanor minimum with $v_T = 3$ and before a drop of high N_2(X, v) density by (V–T) vibration–translation reactions, typically at $v > 35$ as described in [30], we evaluate a γ_v destruction probability of the N_2(X, $v > 3–13$) vibrational levels on the tube walls.

The same procedure as in [31] for N-atoms is taken here for the calculations of the γ_v recombination probability of the N_2(X, $v > 3–13$) molecules on the tube wall.

It is written as follows:

$$[X, v > 3-13]_z = [X, v > 3-13]_{z=0} \cdot \exp[-\upsilon_{X,v} z/v], \quad (7)$$

where $\upsilon_{X,v} = \gamma_v <c>/2R$, <c> is the thermal gas velocity (<c> $= 5 \times 10^4$ cm s^{-1}) and R the tube radius.

$z = 0$ is taken at the RF and HF plasma end, which is at $z = 25$ cm in RF and at $z = 6$ cm in HF, respectively.

For such positions, the flow velocity in the RF set-up can be directly calculated from the gas flow rate and from the tube i.d. (21 mm) for a laminar flow.

From Eq. 7, it is found $\gamma_v = 2 \times 10^{-3}$ after the RF plasma at $z = 25$ cm (residence time of 7×10^{-2} s). At $z > 20$ cm after the HF plasma, it is obtained: $\gamma_v = 5 \times 10^{-3}$ at the residence time of 2×10^{-2} s and $\gamma_v = 3 \times 10^{-3}$ at the residence time of 3.5×10^{-2} s where a laminar flow is expected.

We note that the same range of γ_v values are obtained after the RF and HF plasmas ($\gamma_v = 2–5 \times 10^{-3}$) at long times (7 and 3.5×10^{-3} s) when the parts of LA and PA are in equality.

The present γ_v values are about 2–5 times higher than the previous published value [32] for the first N_2(X, $v = 1$) state: $\gamma_1 = 10^{-3}$ on Pyrex and quartz tube walls. They are largely higher than the γ_N values of N-atoms recombination on quartz and Pyrex tube walls: $\gamma_N = 10^{-5}$–10^{-4} [31]. Such results could come from vibrational relaxation of the N_2(X, v) molecules on the tube wall by $N_2(X, v)$ + wall $\rightarrow N_2(X, v–n)$ +wall, with $n \geq 1$, faster than for the N-atoms with N + wall $\rightarrow$ 1/2 N_2 + wall.

The loss frequency of the N_2(X, $v > 3–13$) on the tube wall is in the range of 50–150 s^{-1}.

It can be compared to the following volume losses: 10 s^{-1} for the reaction $N_2(X, v > 13) + O$ with a rate of 10^{-13} cm^3 s^{-1} [33] with $[O] = 10^{14}$ cm^{-3}; 1–5 s^{-1} for the reaction $N_2(X, v) + N \rightarrow N_2(X, w) + N$, with a rate $k(v = 10–15, w = 0,15) = 1–5 \times 10^{-15}$ cm^3 s^{-1} [34] and $[N] = 10^{15}$ cm^{-3}.

As for the (V–V) and (V–T) collisions, it is given in [35] the characteristic frequencies at 5 Torr, 500 K: $\upsilon(V–V) = 2\ 10^3 s^{-1}$ for $N_2(1) + N_2(0) \rightarrow N_2(0) + N_2(1)$ and $\upsilon(V–T) = 4\ 10^{-3}$ s^{-1} for $N_2(1) + N_2 \rightarrow N_2(0) + N_2$.

Outside the high V–V frequency, these frequencies are low in comparison to the $N_2(X, v > 3–13)$ loss frequency on the tube wall: 50–150 s^{-1}.

Conclusion

To conclude, the presently analyzed N_2 RF and HF flowing plasmas with nearly the same discharge parameters (tube diameters, gas pressure, flow rates and electrical power) produce long time afterglows with about the same N atoms and $N_2(A)$ densities. The main difference between RF and HF appears in the plasma length, which is longer in RF than in HF. As a consequence, the residence time of the active species is increased in the RF plasma, allowing in comparison to HF plasmas an enhancement of $N_2(X, v)$ excitation by (V–V) collisions. Such an effect is detected as a higher density of vibrationally excited $N_2(X, v)$ molecules in the RF plasma and particularly in the afterglow where a pure pink afterglow is observed in RF, 'not in HF'.

If about equal densities of N and $N_2(A)$ are found in the long time RF and HF afterglows, it appears a higher $N_2(X, v > 13)$ and N_2^+ densities in the RF afterglow which can be related to high $N_2(V–V)$ excitation until the plasma end. The present results concern first the N-atom density calibrated by NO titration with an accuracy of 30 %. Then the other active species densities: $N_2(A)$, $N_2(X, v > 13)$ and N_2^+ are obtained by a line-ratio method, giving the order of magnitude of density, depending on kinetic rates of the chosen dominant reactions.

A new result obtained with these RF and HF afterglows concerns the γ_v destruction probability of the $N_2(X, v \geq 3–13)$ vibrational levels on the quartz tube wall, which is more than one order of magnitude higher than for the N-atoms, certainly as the result of a more easy climbing down of $N_2(X, v)$ on the tube wall.

Acknowledgments Y.K.K. acknowledges a financial support from the International Research and Development Program of the National Research Foundation of Korea (NRF) funded by the Ministry of Science, ICT and Future Planning (NRF-2015K1A3A1A21000248). This work was supported by the Franco-Korean project PHC STAR 2015 (34306TK).

References

1. Ricard A, Oh SG, Guerra V (2013) Line-ratio determination of atomic oxygen and N_2 metastable absolute densities in an RF nitrogen late afterglow. Plasma Sources Sci Technol 22(3):035009. doi:10.1088/0963-0252/22/3/035009
2. Zerrouki H, Ricard A, Sarrette JP (2013) Determination of N and O-atom and $N_2(A)$ metastable molecule densities in the afterglows of N_2 and N_2–O_2 microwave discharges. Contrib Plasmas Phys 53(8):599–604. doi:10.1002/ctpp.201300008
3. Ricard A, Oh SG (2014) Densities of active species in N2 and N_2–H_2 RF pink afterglow. Plasma Sources Sci Technol 23(4):045009. doi:10.1088/0963-0252/23/4/045009

4. Zerrouki H, Ricard A, Sarrette JP (2014) Determination of N and O-atoms and N_2-(A) metastable molecule densities in the afterglows of N_2–H_2, Ar–N_2–H_2 and Ar–N_2–O_2 microwave discharges. Contrib Plasmas Phys 54(10):827–837. doi:10.1002/ctpp.201400001
5. Ricard A, Oh SG, Jang J, Kim YK (2015) Quantitative evaluation of the densities of active species of N_2 in the afterglow of Ar-embedded N_2 RF plasma. Curr Appl Phys 15(11):1453–1462. doi:10.1016/j.cap.2015.08.013
6. Philip N, Saoudi B, Crevier MC, Moisan M, Barbeau J, Pelletier J (2002) The respective roles of UV photons and oxygen atoms in plasma sterilization at reduced gas pressure: the case of N_2–O_2 mixtures. IEEE Trans Plasma Sci 30(4):1429–1436. doi:10.1109/TPS.2002.804203
7. Villeger S, Sarrette JP, Ricard A (2005) Synergy between N and O atom action and substrate surface temperature in a sterilization process using a flowing N_2–O_2 microwave post discharge. Plasma Process Polym 2(9):709–714. doi:10.1002/ppap.200500040
8. Pointu A-M, Ricard A, Dodet B, Odic E, Larbre J, Ganciu M (2005) Production of active species in N_2–O_2 flowing post-discharges at atmospheric pressure for sterilization. J Phys D Appl Phys 38(12):1905–1909. doi:10.1088/0022-3727/38/12/009
9. Ricard A, Jaoul C, Gaboriau F, Gherardi N, Villeger S (2004) Production of N, H, O, and C atoms in flowing microwave discharges. Surf Coat Technol 188–189:287–293. doi:10.1016/j.surfcoat.2004.08.171
10. Ricard A, Monna V (2002) Reactive molecular plasmas. Plasma Sources Sci Technol 11(3A):A150. doi:10.1088/0963-0252/11/3A/322
11. Molchan IS, Thompson GE, Skeldon P, Trigoulet N, Chapon P, Tempez A, Malherbe J, Lobo Revilla L, Bordel N, Belenguer P, Nelis T, Zahri A, Therese L, Guillot P, Ganciu M, Michler J, Hohl M (2009) The concept of plasma cleaning in glow discharge spectrometry. J Anal At Spectrom 24(6):734–741. doi:10.1039/B818343K
12. Kaluri SR, Hess DW (1996) Nitrogen incorporation in thin oxides by constant current N_2O plasma anodization of silicon and N_2 plasma nitridation of silicon oxides. Appl Phys Lett 69(8):1053–1055. doi:10.1063/1.116928
13. Ricard A, Hubert J, Michel H (1992) Correlations between active plasma species and steel surface nitriding in microwave post-discharge reactors. In: Capitelli M, Gorse C (eds) Plasma technology: fundamentals and applications. Springer, Boston, pp 125–142. doi:10.1007/978-1-4615-3400-6_9
14. Ricard A, Czerwiec T, Belmonte T, Bockel S, Michel H (1999) Detection by emission spectroscopy of active species in plasma–surface processes. Thin Solid Films 341(1–2):1–8. doi:10.1016/S0040-6090(98)01529-6
15. Zhu X-M, Pu Y-K (2010) Optical emission spectroscopy in low-temperature plasmas containing argon and nitrogen: determination of the electron temperature and density by the line-ratio method. J Phys D Appl Phys 43(40):403001. doi:10.1088/0022-3727/43/40/403001
16. Zerrouki H, Ricard A, Sarrette JP (2014) Determination of N and O-atoms, of N_2 (A) and N_2 (X, $v > 13$) metastable molecules and N^{2+} ion densities in the afterglows of N_2–H_2, Ar–N_2–H_2 and Ar–N_2–O_2 microwave discharges. J Phys Conf Ser 550(1):012045. doi:10.1088/1742-6596/550/1/012045
17. Kang N, Lee M, Ricard A, S-g Oh (2012) Effect of controlled O_2 impurities on N_2 afterglows of RF discharges. Curr Appl Phys 12(6):1448–1453. doi:10.1016/j.cap.2012.04.009
18. Boudam MK, Saoudi B, Moisan M, Ricard A (2007) Characterization of the flowing afterglows of an N_2–O_2 reduced-pressure discharge: setting the operating conditions to achieve a dominant late afterglow and correlating the NO β UV intensity variation with the N and O atom densities. J Phys D Appl Phys 40(6):1694–1711. doi:10.1088/0022-3727/40/6/019
19. Britun N, Gaillard M, Ricard A, Kim YM, Kim KS, Han JG (2007) Determination of the vibrational, rotational and electron temperatures in N_2 and Ar–N_2 RF discharge. J Phys D Appl Phys 40(4):1022. doi:10.1088/0022-3727/40/4/016
20. Nassar H, Pellerin S, Musiol K, Martinie O, Pellerin N, Cormier JM (2004) N_2^+/N_2 ratio and temperature measurements based on the first negative N_2^+ and second positive N_2 overlapped molecular emission spectra. J Phys D Appl Phys 37(14):1904–1916. doi:10.1088/0022-3727/37/14/005
21. Sadeghi N, Foissac C, Supiot P (2001) Kinetics of N_2 ($A\ ^3\Sigma_u^+$) molecules and ionization mechanisms in the afterglow of a flowing N_2 microwave discharge. J Phys D Appl Phys 34(12):1779. doi:10.1088/0022-3727/34/12/304
22. Chaker M, Moisan M, Zakrzewski Z (1986) Microwave and RF surface wave sustained discharges as plasma sources for plasma chemistry and plasma processing. Plasma Chem Plasma Process 6:79–96
23. Massabieaux B, Plain A, Ricard A, Capitelli M, Gorse C (1983) Excitation of vibrational and electronic states in a glow discharge column in flowing N_2. J Phys B At Mol Phys 16(10):1863. doi:10.1088/0022-3700/16/10/021

24. Gordiets B, Hamedov SS, Shelepin IA (1975) Vibrational kinetics of harmonic oscillators under essentially nonequilibrium conditions. Sov Phys JETP 40:640
25. Gilmore FR, Laher RR, Espy PJ (1992) Franck–Condon factors, r-centroids, electronic transition moments, and Einstein coefficients for many nitrogen and oxygen band systems. J Phys Chem Ref Data 21(5):1005–1107. doi:10.1063/1.555910
26. Pancheshnyi SV, Starikovskaia SM, Starikovskii AY (2000) Collisional deactivation of $N_2(C\ ^3\Pi_u, v = 0, 1, 2, 3)$ states by N_2, O_2, H_2 and H_2O molecules. Chem Phys 262(2–3):349–357. doi:10.1016/S0301-0104(00)00338-4
27. De Benedictis S, Dilecce G (1995) Vibrational relaxation of $N_2(C, v)$ state in N_2 pulsed RF discharge: electron impact and pooling reactions. Chem Phys 192(2):149–162. doi:10.1016/0301-0104(94)00370-P
28. Mavadat M, Ricard A, Sarra-Bournet C, Laroche G (2011) Determination of ro-vibrational excitations of N_2 (B, v′) and N_2 (C, v′) states in N_2 microwave discharges using visible and IR spectroscopy. J Phys D Appl Phys 44(15):155207. doi:10.1088/0022-3727/44/15/155207
29. Blanchard H, Sarrette JP, Villeger S, Baudel P, Ricard A (2004) Density of oxygen atoms in high pressure (10–50 torr) flowing microwave post-discharges for elastomer treatments. Eur Phys J Appl Phys 26(03):221–226. doi:10.1051/epjap:2004036
30. Capitelli M, Gorse C, Ricard A (1982) Non equilibrium dissociation and ionization of N_2 in decaying plasmas. J Phys (Paris) 43:L417–L423
31. Villeger S, Sarrette JP, Rouffet B, Cousty S, Ricard A (2008) Treatment of flat and hollow substrates by a pure nitrogen flowing post discharge. Eur Phys J Appl Phys 42(01):25–32. doi:10.1051/epjap:2007177
32. Marinov D, Lopatik D, Guaitella O, Hubner M, Ionikh Y, Ropcke J, Rousseau A (2012) Surface vibrational relaxation of N_2 studied by CO_2 titration with time-resolved quantum cascade laser absorption spectroscopy. J Phys D Appl Phys 45(175201):33
33. Guerra V, Loureiro J (1997) Self-consistent electron and heavy particle kinetics in a low-pressure N_2–O_2 glow discharge. Plasmas Sources Sci Technol 6:373–385
34. Armenise I, Capitelli M, Garcia E, Gorse C, Lagana A, Longo S (1992) Deactivation dynamics of vibrationally excited nitrogen molecules by nitrogen atoms. Chem Phys Lett 200:597–604
35. Capitelli M, Gorse C, Ricard A (1986) Coupling of vibrational and electronic energy distributions in discharge and post-discharge conditions. In: Topics in current chemistry, vol 39. Non equilibrium vibrational kinetics. Chapter 11, pp 315–337